Research Article Vol. 58, No. 6 / 20 February 2019 / Applied Optics 1475

applied optics

Effects of the shape distribution of aerosol particles on their volumetric scattering properties and the radiative transfer through the atmosphere that includes polarization

Li Li,[1] Zhengqiang Li,[1,*] Oleg Dubovik,[2] Xu Zheng,[3] Zhanhua Li,[3] Jinji Ma,[4] and Manfred Wendisch[5]

[1]State Environmental Protection Key Laboratory of Satellite Remote Sensing, Institute of Remote Sensing and Digital Earth, Chinese Academy of Sciences, Beijing 100101, China
[2]Laboratoire d'Optique Atmosphérique, Université de Lille 1/CNRS, Lille 59655, France
[3]State Key Laboratory of Nonlinear Mechanics, Institute of Mechanics, Chinese Academy of Sciences, Beijing 100190, China
[4]College of Territorial Resources and Tourism, Anhui Normal University, Wuhu 241003, China
[5]Leipzig Institute for Meteorology, Leipzig University, Leipzig 04103, Germany
*Corresponding author: lizq@radi.ac.cn

Received 2 October 2018; revised 11 January 2019; accepted 13 January 2019; posted 14 January 2019 (Doc. ID 344951); published 15 February 2019

In this paper, we investigate the effects of shape distribution of aerosol particles on the volumetric scattering properties, as well as the radiance and polarization distributions of skylight, by numerical simulations. The results demonstrate that the shape distribution indeed exerts a significant influence on the skylight degree of linear polarization. The skylight polarization calculated assuming the microscope-measured shape distributions is distinct from that using the inversion-based shape distributions. The significant effects will influence the retrieval of the sphericity of aerosols based on the sun–sky radiometer measurements. Our results suggest that using representative shape distributions obtained by direct microscopic observations of aerosol samples captured in the natural atmosphere has a high potential to improve the retrieval of the aerosol shape parameter.

https://doi.org/10.1364/AO.58.001475

1. INTRODUCTION

Atmospheric aerosol particles modify the radiative energy budget of the Earth–atmosphere system by scattering and absorbing solar radiation [1]. The particle shape has a significant influence on the aerosol light-scattering process. Therefore, the accurate characterization of the particle shape is a key issue for both the realistic representation of light-scattering processes by nonspherical particles (such as dust) to quantify their influence on the energy budget, and for considering the nonsphericity effects in remote-sensing techniques [2,3].

The so-called particle aspect ratio, defined as the ratio of the largest to the smallest particle dimensions [2], quantifies the degree of nonsphericity of aerosol particles. This parameter can be obtained by direct microscopic observation or indirect inversion from light-scattering measurements [4]. The method of direct microscopic observation requires the collection of atmospheric aerosol particles on filters. The particle aspect ratio will then be measured by electron or optical microscopy. Subsequently, the shape distribution, expressed as the aspect ratio number distribution or aspect ratio distribution, is derived as the normalized number of the aspect ratio occurrences of a large sample of individual particles [4].

Okada *et al.* [5] collected mineral dust samples from three arid regions in northern China and measured the average aspect ratios and the shape distributions by electron microscopy. The shape distribution was modeled as the harmonic mean of two exponential functions. Kandler *et al.* [6] collected dust storm samples in Spain. More than 22,000 individual dust particles were analyzed by scanning electron microscopy (SEM), and nearly 200 particles were investigated by transmission electron microscopy (TEM) to obtain representative average shape distributions. A modified lognormal function was applied to parameterize the shape distributions. Kandler *et al.* [7,8] collected samples of dust particles and mixtures of dust and marine aerosols in Morocco and Cape Verde during the Saharan Mineral Dust Experiments (SAMUM) in 2006 and 2008. Based on the modified lognormal model established by Kandler *et al.* [6], the shape distributions of these cases were fitted with high

accuracy. The shape distributions for different size ranges were also given to indicate the dependence of the shape distribution on the particle size [7–9]. Previous studies have concluded that, unlike the aerosol particle size distribution, the shape distributions were relatively stable for different samples of Saharan dusts [8]. The shape distributions measured at different locations during the SAMUM-2008 observations were very similar, and they were also not much different from the earlier measurements conducted during the SAMUM-2006 [8]. Thereby, the shape distributions measured during the SAMUM-2006 were implemented into the new version of the Optical Properties of Aerosols and Clouds (OPAC) 4.0 database as the representative shape distributions of the nonspherical mineral aerosols [7,10].

In the aforementioned studies, electron microscopy techniques were commonly adopted to measure the aerosol shape distribution. The size resolution of SEM scans is better than 1 nm, whereas the one of the TEM technique is even higher (up to 0.1–0.2 nm). Thus, the TEM can be used to observe the structure of tiny particles that cannot be resolved by SEM. However, it is very time consuming to measure tens of thousands of aerosol particles to obtain a statistically significant particle shape distribution with a very high resolution by electron microscopies [4]. Furthermore, previous studies have shown that fine aerosol particles smaller than approximately 500 nm are rather spherical compared to larger particles [7,8]. The characteristics of nonspherical particles with medium or large aspect ratios are more significant for coarse particles. The resolution of some optical microscopes can reach up to tens of nanometers. They can also be applied for observing the coarse-mode dominant nonspherical aerosol particles. Li *et al.* [4] employed a high-resolving fluorescence microscope to observe the coarse-mode dominant aerosol samples collected in northern China. The particle shape distribution was well parameterized by harmonic means of two exponential functions through fitting the aspect ratios of more than 9500 particles.

Inversion techniques based on measurements of scattered light represent an indirect method to obtain the shape information on aerosol particles, in contrast to direct microscopic observations. Some techniques, such as two-dimensional angular optical scattering patterns, acquire shape information by emitting laser radiation and analyzing the angular distribution of the radiance scattered by the nonspherical particles [11,12]. In addition to the active approach, the passive remote sensing can also be applied to derive shape parameters through observing the scattered skylight. One of the typical passive instruments is the ground-based sun–sky radiometer [13,14], which can also be equipped with polarization detection considering that polarization is more sensitive to particle shape in comparison with the total radiance [15,16]. Dubovik *et al.* [15] developed a method to characterize sphericity (i.e., the percentage of spherical particles) from skylight polarization data measured by the sun–sky radiometer operated within the Aerosol Robotic Network (AERONET). The parameter of sphericity or nonsphericity is a simplification for the complex retrieval of shape distribution, where the nonspherical particles are modeled as a mixture of spheres and spheroids with an *a priori* fixed dust shape distribution [15]. The inversion of scattering data measured by the sun–sky radiometer can deliver the shape information of aerosol particles averaged over the entire atmosphere column.

At present, the AERONET operational retrieval algorithm represents the aerosol population as a mixture of spherical and nonspherical aerosol fractions. The shape distribution of particles in nonspherical components is fixed *a priori* to the shape distribution, which is derived from the laboratory measurements of scattered light [15,17]. Such a strategy didn't show any evident deficiency, and it was therefore also applied in numerous satellite retrieval algorithms [18,19]. At the same time, there are only very limited efforts regarding the investigation of potential limitations, as well as uncertainties that could be related with the deviation of the assumed shape distribution from real ones. Indeed, the fitting [15] was done for phase matrices measured in the laboratory for Feldspars dust samples originating from soil and proceeded into fine powder [17]. Those particles were not directly sampled from the atmosphere [17] and therefore were unlikely to realistically represent the diversity of the ambient dust particle distribution. For example, the derived shape distribution of Feldspar samples showed different features compared to the atmospheric dust shape distributions measured by direct microscopic observations [4–6,8,20]. Thus, although the measurements of atmospheric radiance and linear polarization can apparently be well fitted by using the fixed dust shape distribution [15,21], and the sensitivity of retrieval to details of shape distribution is often limited [15], the fundamental uncertainty associated with the fixed single shape distribution in the retrieval remains and needs to be thoroughly investigated.

Different aerosol particle shape distributions may modify the volumetric scattering properties and the radiative transfer through the atmosphere, and then affect the retrieval of the shape parameter from the skylight measurements. A discussion on the effects of aerosol particle shape distributions derived from diverse approaches on the polarization of skylight will help to improve the retrievals of the sphericity parameter and other simultaneously derived aerosol properties, and it will further improve the estimation of nonspherical aerosol radiative forcing. In this study, the effects of different aerosol shape distributions on the aerosol volumetric optical properties (e.g., volumetric extinction coefficient, scattering coefficient, single scattering albedo, and scattering matrix) and the distributions of the total radiance, the degree of linear polarization, and the angle of polarization of skylight in the celestial hemisphere are analyzed by numerical simulations. The aim is to discuss how much the calculation of skylight polarization is affected by the different shape distribution assumptions obtained from direct microscopical observations, or the commonly used hypothetical distributions with respect to the *a priori* dust shape distribution adopted in the sun–sky radiometer retrievals.

2. PARAMETERIZATION OF THE AEROSOL PARTICLE SHAPE DISTRIBUTION

The aerosol particles in the atmosphere are characterized by a wide variety of shapes that makes it a challenge to model the natural atmospheric aerosols accurately [4]. Although many complex shape types (e.g., Chebyshev particles with rough surfaces, porous particles, aggregates) have been successfully assumed in fundamental light-scattering studies, the application

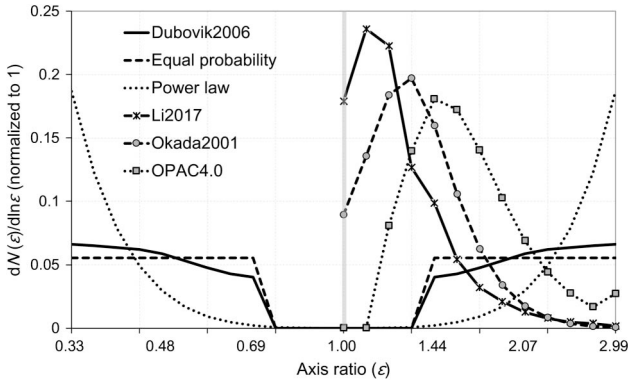

Fig. 1. Six different particle shape distributions of atmospheric aerosols adopted in simulation. The Li2017, Okada2001, and OPAC4.0 shape distributions are unilateral distributions; the Dubovik2006, equal probability, and power law shape distributions are bilateral distributions with an equal presence of oblate and prolate spheroids with the same axis ratios [15].

of the highly simplified spheroid model is preferable, because it is more practical for aerosol remote-sensing techniques [2,3,15,16,22]. Only one shape parameter (i.e., the aspect ratio or axis ratio) needs to be additionally considered for the randomly oriented polydisperse spheroids compared with spherical particles [15]. Previous research has shown that the spheroidal shape model with a mixture of spheres and spheroids with different aspect ratios has obvious advantages in describing the volumetric optical properties of nonspherical particles in the atmosphere [23,24]. Thus, the spheroid and corresponding shape distribution of the particle dispersion are adopted to model the optical properties of a volume of atmospheric particles in this study. In case of a spheroid model, the shape distribution corresponds to the axis ratio distribution of the particle population $\mathrm{d}N(\varepsilon)/\mathrm{d}\ln(\varepsilon)$, with N being the number of particles for a specified axis ratio ε. The axis ratio represents the ratio of the rotational semi-axis to the horizontal semi-axis of the spheroid [15]. It is equal to the aspect ratio for the prolate spheroid (i.e., $\varepsilon > 1$).

Several shape distributions, including the fixed one for dust particles derived from light-scattering measurements (i.e., Dubovik2006) [15], three shape distributions obtained by direct microscopy (i.e., Li2017, Okada2001, and OPAC4.0) [4,5,10], as well as two commonly applied hypothetical aerosol shape distributions (i.e., equal probability and power law distributions) [2,15,25–27], have been used (Fig. 1). Among them, the Li2017, Okada2001, and OPAC4.0 distributions [4,5,10] consider prolate spheroids only (i.e., $\varepsilon > 1$), whereas both cases of prolate and oblate spheroids (i.e., $\varepsilon > 1$ and $0 < \varepsilon < 1$) are applied in the Dubovik2006 [15], the equal probability, and the power law distributions [2,15,25–27]. The six shape distributions are normalized to 1.

3. SIMULATIONS OF VOLUMETRIC OPTICAL PROPERTIES AND SKYLIGHT POLARIZATION

A. Volumetric Optical Properties of Spheroids

The conversion from incident to scattered radiation through light scattering of randomly oriented spheroid particles can be described by the Stokes vectors and the scattering matrix as [1,15,17,25]

$$\begin{pmatrix} I' \\ Q' \\ U' \\ V' \end{pmatrix} \propto \begin{bmatrix} F_{11}(\Theta) & F_{12}(\Theta) & 0 & 0 \\ F_{12}(\Theta) & F_{22}(\Theta) & 0 & 0 \\ 0 & 0 & F_{33}(\Theta) & F_{34}(\Theta) \\ 0 & 0 & -F_{34}(\Theta) & F_{44}(\Theta) \end{bmatrix} \begin{pmatrix} I \\ Q \\ U \\ V \end{pmatrix}, \tag{1}$$

where $(I, Q, U, V)^{\mathrm{T}}$ and $(I', Q', U', V')^{\mathrm{T}}$ are the Stokes vectors of incident and scattered radiation, respectively. The superscript T indicates transposition. F_{11}, F_{12}, F_{22}, F_{33}, F_{34}, and F_{44} are the six angular-dependent nonzero elements of the scattering matrix. Θ represents the scattering angle that is defined as the angle between the directions of incident and scattered radiation within the scattering plane.

The Mie theory is applicable to the scattering of homogeneous spherical particles [28–30]. For nonspherical, randomly oriented spheroids, other approaches such as the T-matrix, discrete dipole approximation, and geometric optics methods have often been used to calculate the light scattering by spheroids with different particle sizes and axis ratios [31–33]. The volumetric optical properties of spheroids with specific particle size and shape distributions are obtained by integration of the single scattering properties [1,15,16].

Assuming that the aerosol shape distribution is the same at different particle sizes, the integrated volumetric properties (extinction and scattering coefficients, i.e., $\langle b_{\mathrm{ext}}(\lambda)\rangle$ and $\langle b_{\mathrm{sca}}(\lambda)\rangle$) are obtained from the weighted volume size distribution and shape distribution as [1,2,15,16]

$$\langle b_{\mathrm{ext}}(\lambda)\rangle = \int_{\ln \varepsilon_{\min}}^{\ln \varepsilon_{\max}} \int_{\ln r_{\min}}^{\ln r_{\max}} \frac{C_{\mathrm{ext}}(\lambda, \varepsilon, r)}{v(r)} \cdot \frac{\mathrm{d}N(\varepsilon)}{\mathrm{d}\ln \varepsilon} \frac{\mathrm{d}V(r)}{\mathrm{d}\ln r} \mathrm{d}\ln r \mathrm{d}\ln \varepsilon, \tag{2}$$

$$\langle b_{\mathrm{sca}}(\lambda)\rangle = \int_{\ln \varepsilon_{\min}}^{\ln \varepsilon_{\max}} \int_{\ln r_{\min}}^{\ln r_{\max}} \frac{C_{\mathrm{sca}}(\lambda, \varepsilon, r)}{v(r)} \cdot \frac{\mathrm{d}N(\varepsilon)}{\mathrm{d}\ln \varepsilon} \frac{\mathrm{d}V(r)}{\mathrm{d}\ln r} \mathrm{d}\ln r \mathrm{d}\ln \varepsilon, \tag{3}$$

where the brackets $\langle \ldots \rangle$ denote the volumetric optical properties [1]. C_{ext} and C_{sca} are the extinction and scattering cross sections, respectively. λ is the wavelength, ε is the axis ratio, and r is the radius. $v(r)$ denotes the particle volume with a radius of r. $\mathrm{d}N(\varepsilon)/\mathrm{d}\ln \varepsilon \mathrm{d}N(\varepsilon)/\mathrm{d}\ln \varepsilon$ and $\mathrm{d}V(r)/\mathrm{d}\ln r$ represent the shape distribution and the volume size distribution of spheroidal particles, respectively. The ranges of the particle size and the axis ratio for integration are consistent with the inversion algorithm of the sun–sky radiometer (i.e., the particle sizes range from 0.05 μm to 15 μm, and the axis ratios range from 0.3 to 3.0).

In a similar manner, the integrated, volumetric single scattering albedo $\langle \varpi(\lambda)\rangle$ can be calculated as

$$\langle \varpi(\lambda)\rangle = \frac{\int_{\ln \varepsilon_{\min}}^{\ln \varepsilon_{\max}} \int_{\ln r_{\min}}^{\ln r_{\max}} \frac{\varpi(\lambda, \varepsilon, r) \cdot C_{\mathrm{ext}}(\lambda, \varepsilon, r)}{v(r)} \cdot \frac{\mathrm{d}N(\varepsilon)}{\mathrm{d}\ln \varepsilon} \frac{\mathrm{d}V(r)}{\mathrm{d}\ln r} \mathrm{d}\ln r \mathrm{d}\ln \varepsilon}{\langle b_{\mathrm{ext}}(\lambda)\rangle}. \tag{4}$$

The angular-dependent elements of the volumetric scattering matrix are calculated as

$$\langle F_{ij}(\lambda,\Theta)\rangle = \frac{\int_{\ln \varepsilon_{\min}}^{\ln \varepsilon_{\max}} \int_{\ln r_{\min}}^{\ln r_{\max}} \frac{F_{ij}(\lambda,\Theta,\varepsilon,r)\cdot C_{\mathrm{sca}}(\lambda,\varepsilon,r)}{v(r)} \cdot \frac{\mathrm{d}N(\varepsilon)}{\mathrm{d}\ln \varepsilon}\frac{\mathrm{d}V(r)}{\mathrm{d}\ln r}\mathrm{d}\ln r \mathrm{d}\ln \varepsilon}{\langle b_{\mathrm{sca}}(\lambda)\rangle}, \tag{5}$$

where $i,j = 1,2,3,4$ corresponding to the subscripts of six nonzero elements of the scattering matrix. The spheroid kernel database precalculated by the T-matrix and geometric optics methods was employed to simulate the volumetric optical properties [15,16]. The results of the scattering function F_{11} are normalized to 1 at the scattering angle of 30° to facilitate comparisons with the laboratory measurements and other light-scattering calculations [17]. The remaining five nonzero elements of the scattering matrix are shown relative to the corresponding scattering function [17].

B. Simulation of Skylight Polarization

The skylight becomes partially polarized after the interactions of the nonpolarized solar radiation incident at the top of the atmosphere with the molecules, aerosol particles, water droplets, ice crystals, and precipitation elements in the atmosphere. The component of circular polarization of skylight can often be neglected [34]. Hence, the polarization characteristics of skylight are described by the total radiance I, the degree of linear polarization DoLP, and the angle of polarization AoP. The DoLP and AoP can be calculated as

$$\mathrm{DoLP} = \frac{\sqrt{Q^2+U^2}}{I}, \tag{6}$$

$$\mathrm{AoP} = \frac{1}{2}\mathrm{atan}\frac{U}{Q}. \tag{7}$$

In this paper, the skylight polarization in the celestial hemisphere is simulated by the successive order of scattering (SOS) vector radiation transfer model [35]. The input parameters adopted in the simulation are listed in Table 1. The volumetric optical properties of spheroids assuming different shape distributions calculated in the previous step are put into the SOS model to simulate the radiative transfer through the atmosphere. The output of the first three components of the Stokes vector of skylight are normalized by the extraterrestrial solar irradiance F_0 (i.e., $\pi I/F_0$, $\pi Q/F_0$, and $\pi U/F_0$). Then, the degree of linear polarization and the angle of polarization are derived from the normalized I, Q, and U.

Table 1. Input Parameters Adopted in Simulation

Parameter	Value
Wavelength (λ)	0.44 μm
Particle size distribution ($\mathrm{d}V/\mathrm{dln}r$)	Bi-model lognormal size distribution for background dust [36]
Particle shape distribution ($\mathrm{d}N/\mathrm{dln}\varepsilon$)	Dubovik2006 [15] Equal probability [15] Power law [26] Li2017 [4] Okada2001 [5] OPAC4.0 ($r > 0.5$ μm) [10]
Refractive index (m)	$1.566 + 0.007i$ [7]
Aerosol optical depth	0.2785 [36]
Molecular optical depth	0.243
Solar zenith angle	45°
Surface albedo	0.15

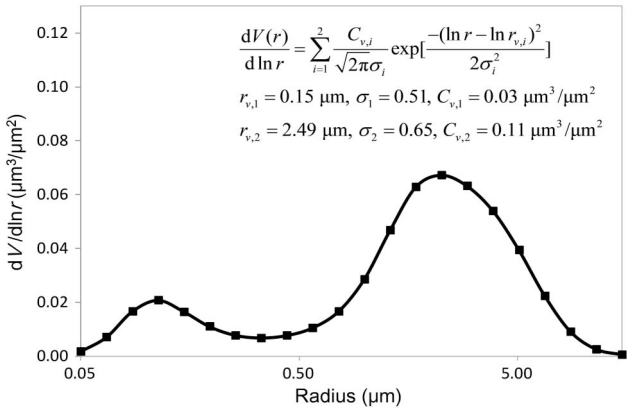

Fig. 2. Bi-model lognormal size distribution for background dust aerosols [36].

The aerosol optical thickness and the volume size distribution are the multi-year average values based on long-term measurements at the typical desert station Minqin within the Sun–Sky Radiometer Observation Network (SONET, www.sonet.ac.cn) from 2012 to 2016, see Fig. 2 [36]. The volume size distribution at Minqin is a representative distribution of background dust dominated by coarse-mode particles, which is similar to size distributions at the adjacent Zhangye site and in the clear case of the Beijing-RADI site of SONET [4,36]. The volume-weighted, effective complex refractive index derived from chemical measurements at Tinfou, Morocco, is adopted as the typical dust refractive index, considering that multiple chemical measurements have reported a real part of the dust refractive index larger than the one commonly retrieved from the sun–sky radiometer and adopted in the basic dust aerosol model (e.g., 1.53) [7,8,37,38].

4. RESULTS

A. Effects of the Particle Shape Distribution on Aerosol Volumetric Optical Properties

The volumetric optical properties, including the extinction and scattering coefficients, as well as the single scattering albedo for aerosol particles with different particle shape distributions, are listed in Table 2. It appears that the changes in particle shape distributions have little effect on the volumetric extinction (less than 3.5%) and scattering (less than 4%) coefficients, as well as on the single scattering albedo (less than 0.6%). Although the particle shape distributions change significantly (see Fig. 1), the maximum difference in the volumetric single scattering albedo is only 0.0052. The volumetric extinction and scattering coefficients show similar variations with the changes of different particle shape distributions. The maximum differences for $\langle b_{\mathrm{ext}}(\lambda)\rangle$ and $\langle b_{\mathrm{sca}}(\lambda)\rangle$ are 0.0112 m^{-1} and 0.0117 m^{-1}, respectively. Therefore, the influences of different particle shape distributions on the aerosol particle volumetric extinction and

Table 2. Extinction Coefficient, Scattering Coefficient, and Single Scattering Albedo of a Volume of Aerosol Particles with Different Shape Distributions

Aerosol Shape Distribution	Volumetric Optical Properties		
	$\langle b_{ext}(\lambda)\rangle(m^{-1})$	$\langle b_{sca}(\lambda)\rangle(m^{-1})$	$\langle \varpi(\lambda)\rangle$
Dubovik2006	0.3302	0.2980	0.9026
Equal probability	0.3295	0.2972	0.9021
Power law	0.3345	0.3029	0.9054
Li2017	0.3233	0.2912	0.9005
Okada2001	0.3237	0.2914	0.9002
OPAC4.0	0.3252	0.2930	0.9008

scattering coefficients, as well as on single scattering albedo, are negligible in the cases studied here.

The effects of different shape distributions on the six independent, nonzero elements of the aerosol particle scattering matrix are illustrated in Fig. 3. It is apparent that the changes of the normalized scattering function F_{11}/F_{11} (30°) with different particle shape distributions are small. More obvious differences for F_{11}/F_{11} (30°) appear at the scattering angles from 150° to 180° in comparison with the forward and sideward scattering directions. The particle shape distributions have a modest impact on F_{33}/F_{11} and F_{44}/F_{11}. The extents and trends of variations for F_{33}/F_{11} and F_{44}/F_{11} are similar, assuming the same particle shape distribution. That is, F_{33}/F_{11} and F_{44}/F_{11} for the Li2017 and the Okada2001 distributions have larger values; the curves for the power law shape distribution have lower values; and the values for other shape distributions are in the middle at most of the scattering angles from 0° to 180°. Conversely, the effects of the particle shape distributions are pronounced with respect to $-F_{12}/F_{11}$, F_{22}/F_{11}, and F_{34}/F_{11}. Among them, the curves of $-F_{12}/F_{11}$ and F_{34}/F_{11} change gradually with different shape distributions. The largest difference occurs between the curves of Li2017 and power law shape distributions at most of the scattering angles. Moreover, the differences between the unilateral distributions (i.e., Li2017, Okada2001, and OPAC4.0) and the bilateral distributions (i.e., Dubovik2006, equal probability, and the power law distributions) are obvious for $-F_{12}/F_{11}$, F_{22}/F_{11}, and

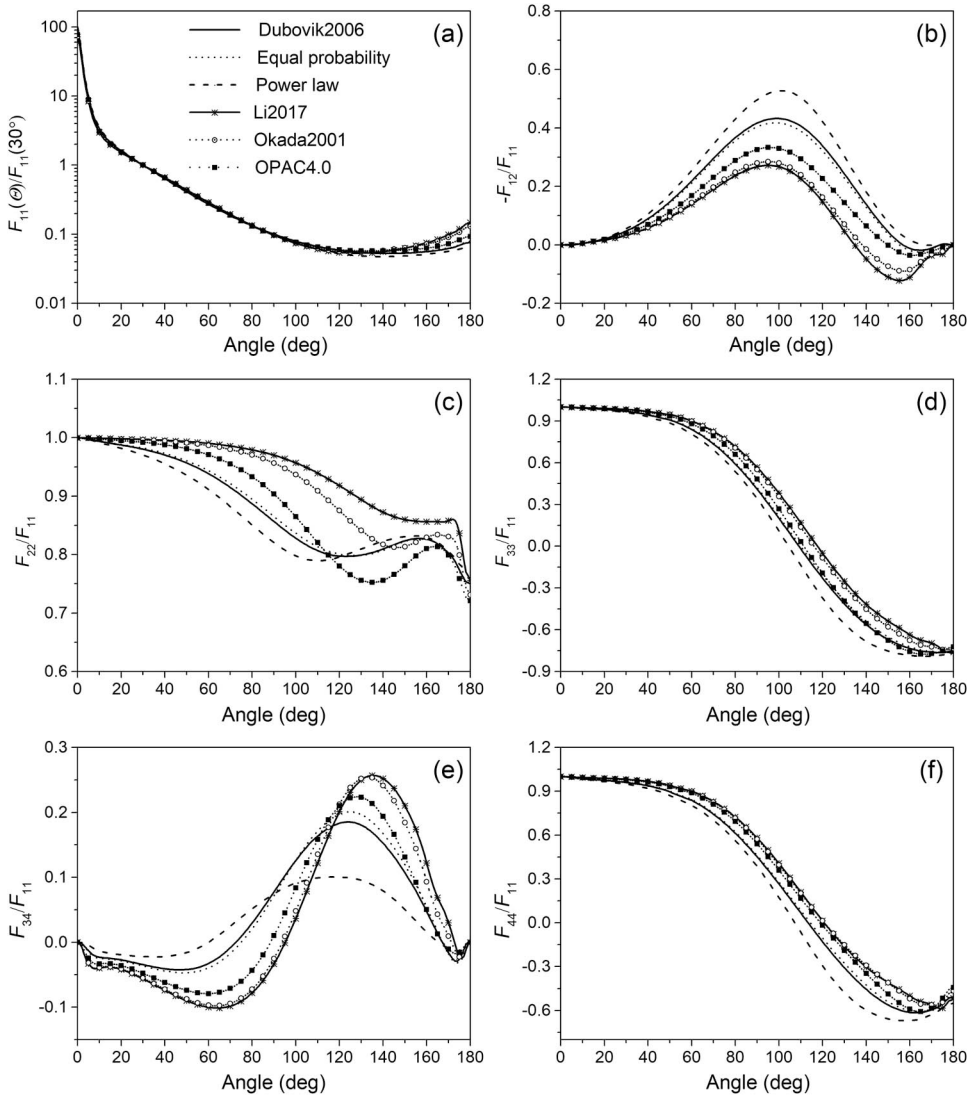

Fig. 3. Independent non-zero elements of scattering matrix for atmospheric aerosols with different particle shape distributions.

F_{34}/F_{11}. It is associated with the fact that the weights of the particles with extreme axis ratios are large in the bilateral distributions, while the unilateral distributions are dominated by the particles close to sphere (see Fig. 1). According to Eq. (1), the changes of $-F_{12}/F_{11}$ and F_{22}/F_{11} can contribute to the measurements of linear polarization for the passive remote sensing of the sun–sky radiometer with the unpolarized incident light and the active remote sensing of Lidar with linearly polarized incident light. Therefore, the influences of different shape distributions on the measurements of skylight polarization are not negligible.

In general, the elements of the scattering matrix calculated by the Li2017 scenario and the Okada2001 distribution based on direct microscopy are close, which is possibly because the sampling regions are all in northern China [4,5]. The elements of the scattering matrix calculated by the Dubovik2006 distribution and the hypothetical equal probability distribution are almost equivalent, which is consistent with the results from previous research [15]. Correspondingly, the curves calculated with the OPAC4.0 shape distribution based on direct microscopic measurements of the Sahara dust samples are in the middle. However, the curves calculated with the hypothetical power law distribution deviate from the results of other distributions. As can be seen in Figs. 1 and 3, the curves of scattering matrix calculated with more similar distributions are closer. Meanwhile, the shape distributions for the samples collected

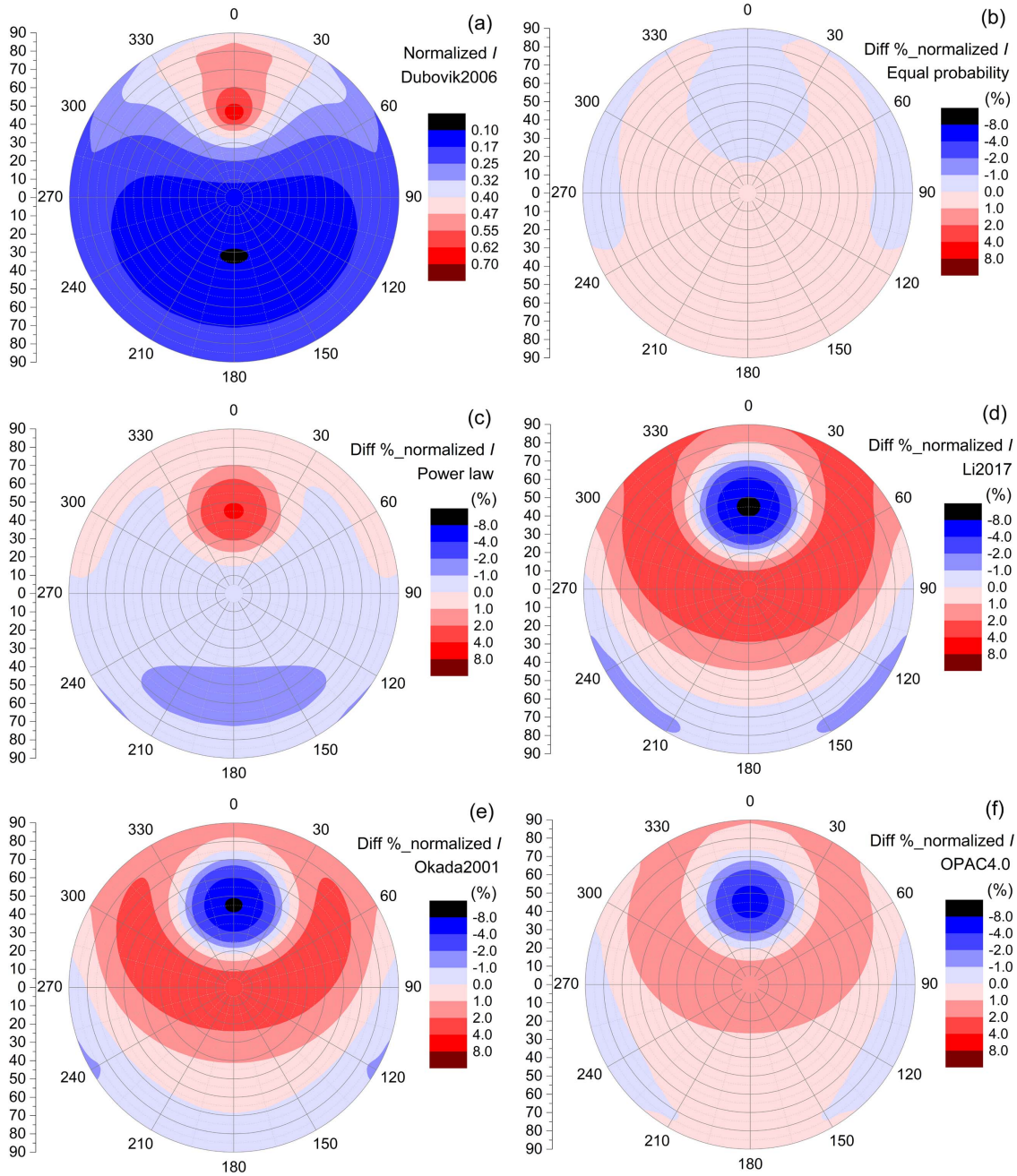

Fig. 4. Effects of aerosol shape distribution on the normalized radiance I of skylight in the celestial hemisphere.

in the same region (e.g., Li2017 and Okada2001) have similar features. Consequently, representative dust-like aerosol shape distributions could be obtained by multiple measurements in different typical regions, which can be applied in the light-scattering calculation of nonspherical aerosols.

B. Effects of Particle Shape Distribution on Skylight Polarization in the Celestial Hemisphere

The normalized total radiance of skylight in the celestial hemisphere assuming the Dubovik2006 distribution, as well as the percentage changes of the normalized radiance under other aerosol shape distributions relative to that of the Dubovik2006 distribution, are presented in Fig. 4. It is evident that the normalized radiance in the case of equal probability distribution is very close to that of Dubovik2006, with tiny relative changes of only ±1% in the entire hemisphere. However, the relative changes are obvious for other shape distributions with respect to the case of the Dubovik2006 distribution. The percentage changes corresponding to the power law distribution are positive near the solar incident direction (i.e., SZA = 45° and the relative azimuthal angle RAA = 0°). They vary from positive to negative with an increasing scattering angle. Conversely, the percentage changes corresponding to the distributions of Li 2017, Okada2001, and OPAC4.0 are negative near the solar incident direction. They vary from negative to positive with an increasing scattering angle, and they change to negative again in some directions with the scattering angles exceeding

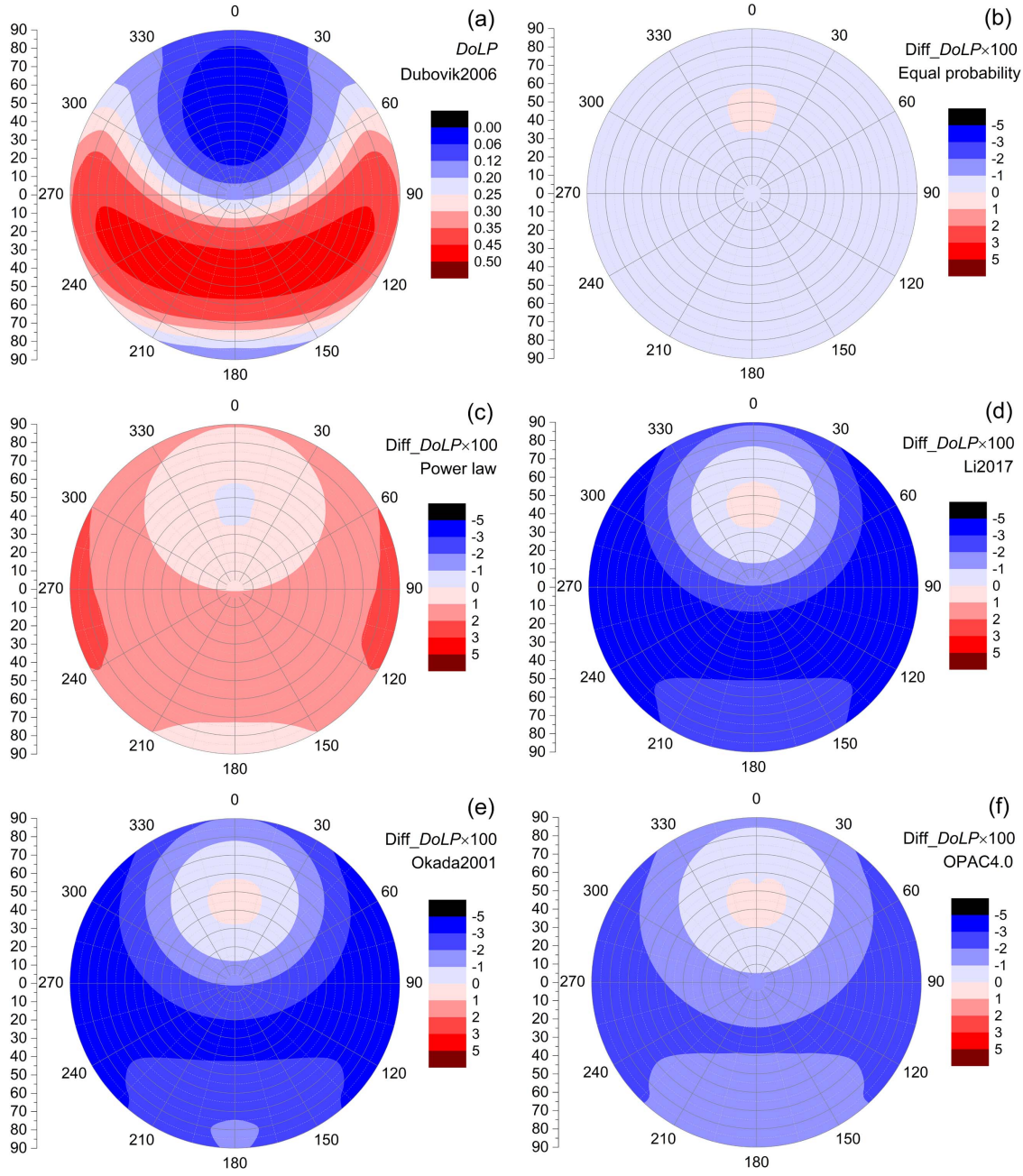

Fig. 5. As Fig. 4, but for the degree of linear polarization of skylight.

approximately 80° ~ 115°. The maximum absolute percentage change is over 8% for the three cases, which appears near the solar incident direction. Generally, the normalized radiances assuming the Li2017 and the Okada2001 distributions are more significantly different from those with the Dubovik2006 distribution; the relative changes of the equal probability and the power law distributions are smaller; and the change of the OPAC4.0 distribution is in the middle.

Figure 5 depicts the degree of linear polarization of skylight in the celestial hemisphere assuming the Dubovik2006 shape distribution, as well as the differences of DoLP under other aerosol shape distributions relative to that of the Dubovik2006 distribution. Similar to the situation of the normalized radiance, DoLP assuming the equal probability distribution is not much different from that of the Dubovik2006 distribution, with differences within ±0.01 in the entire hemisphere. DoLP of skylight under the distribution of power law is greater than that of the Dubovik2006 distribution in the celestial hemisphere, except for the angles around the solar incident direction. In contrast, the values of DoLP under the Li2017, Okada2001, and OPAC4.0 distributions are remarkably less than those under the Dubovik2006 distribution in the celestial hemisphere, with the exception of angles around the solar incident direction. The maximum absolute difference is up to 0.05. Although the maximum differences of the DoLP for the distributions of Li2017, Okada2001, and OPAC4.0 mainly occur near the scattering angle of 90°, the relative changes are exceeding 20% in many observation directions. Therefore, the degree of linear polarization is generally more sensitive to the changes of aerosol shape distributions in comparison with the normalized total radiance of skylight in the celestial hemisphere.

Figure 6 gives the corresponding results of the angle of polarization. From Fig. 6(a), an obvious feature of the AoP of skylight is that the angles of polarization are all equal to 90° in the solar principal plane (i.e., the plane containing both the directions of incident sunlight and the local zenith), except for the angles around the solar incident direction. Apart from these angles, the differences of AoP for other aerosol shape distributions with respect to the distribution of Dubovik2006 are all equal to 0 in the solar principal plane, which means that AoP of skylight in the principal plane does not change with the aerosol shape distribution. Meanwhile, the changes of AoP in other observation angles outside the principal plane are also not significant, with the angle differences mostly within ±0.5°. The large differences appear at the relative azimuthal angles of approximately 0° ~ 45° and 315° ~ 360° for the shape distributions of Li2017 and Okada2001 [see Figs. 6(d) and 6(e)]. It also should be noted that the errors resulting from the inter-angle interpolation in the celestial hemisphere lead to some false irregular changes of AoP.

5. SUMMARY AND CONCLUSIONS

An *a priori* fixed shape distribution of dust particles has widely been applied in the inversion of aerosol particle properties based on measurements collected with the sun–sky radiometers. This dust particle shape distribution derived from laboratory measurements shows different features compared to results obtained by direct microscopic observations of aerosol particle samples captured in the natural atmosphere. Therefore, we compared the optical effects of the dust shape distribution (i.e., Dubovik2006) with three shape distributions obtained by direct microscopic observations (i.e., Li2017, Okada2001, and OPAC4.0). Furthermore, two common hypothetical particle shape distributions (i.e., equal probability and power law distributions) were considered in the comparison.

The sensitivities of the aerosol volumetric extinction and scattering coefficients, single-scattering albedo, and the independent nonzero elements of the scattering matrix to the particle shape distribution were discussed. The results of numerical simulations illustrate that the influences of different particle shape distributions on the integrated volumetric properties (aerosol volumetric extinction coefficient, scattering coefficient, and single scattering albedo) are small. However, the effects of particle shape distributions on the angular-dependent, volumetric elements of the scattering matrix are distinct. Among them, the influences on the normalized volumetric scattering function F_{11}/F_{11} (30°) are not significant, except for the scattering angles from 150° to 180°. F_{33}/F_{11} and F_{44}/F_{11} moderately vary with the changes of the particle shape distributions. In contrast, the particle shape distribution has a pronounced influence on $-F_{12}/F_{11}$, F_{22}/F_{11}, and F_{34}/F_{11}.

In a second step, the impacts of the particle shape distribution on the angular radiance distribution and polarization properties of the skylight (including multiple scattering effects simulated by a radiative transfer model) were quantified. In particular, the differences in the normalized total radiance, the degree of linear polarization, and the angle of polarization of skylight in the celestial hemisphere were analyzed assuming different particle shape distributions. The simulations indicate that relative changes of the normalized radiance for the hypothetical equal probability and the power law particle shape distributions with respect to the fixed dust shape distribution (i.e., Dubovik2006) can be neglected. However, the effects become remarkable for the three particle shape distributions obtained by direct microscopic observations. The maximum absolute percentage change is greater than 8%. Compared with the normalized radiance, the degree of linear polarization of skylight is more sensitive to the changes of aerosol particle shape distributions. The differences in DoLP for the shape distributions obtained by three direct microscopic observations can exceed 20% with respect to the case when the Dubovik2006 distribution is assumed. In contrast, the particle shape distribution has almost no influence on the angle of skylight polarization. The angle differences are mostly within ±0.05° in the celestial hemisphere. Moreover, the angle of polarization does not change with the aerosol shape distribution in the principal plane, except for the angles around the solar incident direction.

The simulations reveal that the particle shape distribution has a significant influence on the degree of linear polarization of skylight. The *a priori* fixed dust shape distribution adopted in the current inversion algorithm of the sun–sky radiometer exerts a similar effect on skylight polarization as the hypothetical equal probability distribution, but it presents larger differences with respect to the particle shape distributions

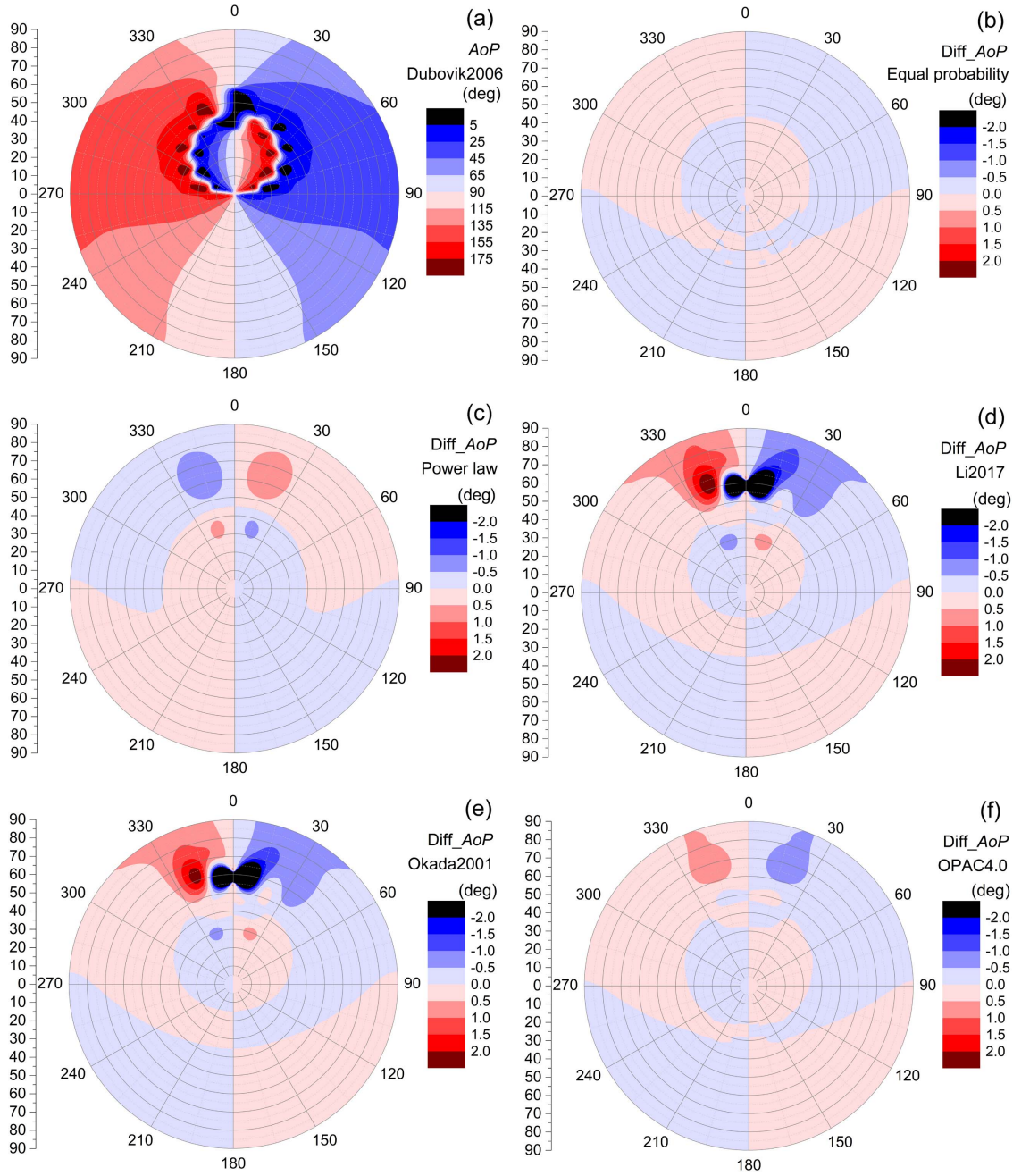

Fig. 6. As Fig. 4, but for the angle of polarization of skylight.

obtained by direct microscopic observations. That could be a critical factor affecting the inversion of sphericity from the sun–sky radiometer measurements. In addition, the results demonstrate that the polarization of skylight assuming the Li2017 and Okada2001 particle shape distributions obtained by microscopic measurements in northern China are close to each other. Thereby, it can be expected to obtain the representative dust-like aerosol particle shape distributions through multiple measurements by direct microscopy in different typical regions. In future research, a database of light-scattering properties of nonspherical aerosol particles should be complemented by typical directly measured particle shape distributions to improve the retrievals of sphericity and corresponding microphysical parameters (e.g., refractive index and particle size distribution) of aerosol particles from the skylight polarization measurements by the sun–sky radiometer.

Funding. National Natural Science Foundation of China (NSFC) (41871271, 41501390, 41671364); Science and Technology Service network initiative (STS) Project of Chinese Academy of Sciences (CAS) (KFJ-STS-QYZD-022).

REFERENCES

1. M. Wendisch and P. Yang, *Theory of Atmospheric Radiative Transfer: a Comprehensive Introduction* (Wiley-VCH, 2012).

2. M. I. Mishchenko, L. D. Travis, R. A. Kahn, and R. A. West, "Modeling phase functions for dustlike tropospheric aerosols using a shape mixture of randomly oriented polydisperse spheroids," J. Geophys. Res. Atmos. **102**, 16831–16847 (1997).
3. S. Merikallio, H. Lindqvist, T. Nousiainen, and M. Kahnert, "Modelling light scattering by mineral dust using spheroids: assessment of applicability," Atmos. Chem. Phys. **11**, 5347–5363 (2011).
4. L. Li, X. Zheng, Z. Q. Li, Z. H. Li, O. Dubovik, X. F. Chen, and M. Wendisch, "A new fluorescence microscopy method to study aerosol shape distribution and its application in modeling light scattering," Opt. Express **25**, A815 (2017).
5. K. Okada, J. Heintzenberg, K. Kai, and Y. Qin, "Shape of atmospheric mineral particles collected in three Chinese arid-regions," Geophys. Res. Lett. **28**, 3123–3126 (2001).
6. K. Kandler, N. Benker, U. Bundke, E. Cuevas, M. Ebert, P. Knippertz, S. Rodriguez, L. Schutz, and S. Weinbruch, "Chemical composition and complex refractive index of Saharan mineral dust at Izana, Tenerife (Spain) derived by electron microscopy," Atmos. Environ. **41**, 8058–8074 (2007).
7. K. Kandler, L. Schutz, C. Deutscher, M. Ebert, H. Hofmann, S. Jackel, R. Jaenicke, P. Knippertz, K. Lieke, and A. Massling, "Size distribution, mass concentration, chemical and mineralogical composition and derived optical parameters of the boundary layer aerosol at Tinfou, Morocco, during SAMUM 2006," Tellus B **61**, 32–50 (2009).
8. K. Kandler, K. Lieke, N. Benker, C. Emmel, M. Kupper, D. Mullerebert, M. Ebert, D. Scheuvens, A. Schladitz, and L. Schutz, "Electron microscopy of particles collected at Praia, Cape Verde, during the Saharan mineral dust experiment: particle chemistry, shape, mixing state and complex refractive index," Tellus B **63**, 475–496 (2011).
9. M. Wiegner, J. Gasteiger, K. Kandler, B. Weinzierl, K. Rasp, M. Esselborn, V. Freudenthaler, B. Heese, C. Toledano, and M. Tesche, "Numerical simulations of optical properties of Saharan dust aerosols with emphasis on lidar applications," Tellus **61**, 180–194 (2009).
10. P. Koepke, J. Gasteiger, and M. Hess, "Technical note: optical properties of desert aerosol with non-spherical mineral particles: data incorporated to OPAC," Atmos. Chem. Phys. **15**, 5947–5956 (2015).
11. K. B. Aptowicz, R. G. Pinnick, S. C. Hill, Y. L. Pan, and R. K. Chang, "Optical scattering patterns from single urban aerosol particles at Adelphi, Maryland, USA: A classification relating to particle morphologies," J. Geophys. Res. **111**, D12212 (2006).
12. K. B. Aptowicz, Y. L. Pan, S. D. Martin, E. Fernandez, R. K. Chang, and R. G. Pinnick, "Decomposition of atmospheric aerosol phase function by particle size and asphericity from measurements of single particle optical scattering patterns," J. Quant. Spectrosc. Radiat. Transfer **131**, 13–23 (2013).
13. M. Wendisch and W. Von Hoyningen-Huene, "Possibility of refractive index determination of atmospheric aerosol particles by ground-based solar extinction and scattering measurements," Atmos. Environ. **28**, 785–792 (1994).
14. L. Li, Z. Q. Li, K. T. Li, L. Blarel, and M. Wendisch, "A method to calculate Stokes parameters and angle of polarization of skylight from polarized CIMEL sun/sky radiometers," J. Quant. Spectrosc. Radiat. Transfer **149**, 334–346 (2014).
15. O. Dubovik, A. Sinyuk, T. Lapyonok, B. N. Holben, M. I. Mishchenko, P. Yang, T. F. Eck, H. Volten, O. Munoz, and B. Veihelmann, "Application of spheroid models to account for aerosol particle nonsphericity in remote sensing of desert dust," J. Geophys. Res. Atmos. **111**, D11208 (2006).
16. O. Dubovik, B. N. Holben, T. Lapyonok, A. Sinyuk, M. I. Mishchenko, P. Yang, and I. Slutsker, "Non-spherical aerosol retrieval method employing light scattering by spheroids," Geophys. Res. Lett. **29**, 1–4 (2002).
17. H. Volten, O. Muñoz, E. Rol, J. F. de Haan, W. Vassen, J. W. Hovenier, K. Muinonen, and T. Nousiainen, "Scattering matrices of mineral aerosol particles at 441.6 nm and 632.8 nm," J. Geophys. Res. **106**, 17375–17401 (2001).
18. O. Dubovik, M. Herman, A. Holdak, T. Lapyonok, D. Tanré, J. L. Deuzé, F. Ducos, A. Sinyuk, and A. Lopatin, "Statistically optimized inversion algorithm for enhanced retrieval of aerosol properties from spectral multi-angle polarimetric satellite observations," Atmos. Meas. Tech. **4**, 975–1018 (2011).
19. O. P. Hasekamp and J. Landgraf, "Retrieval of aerosol properties over land surfaces: capabilities of multiple-viewing-angle intensity and polarization measurements," Appl. Opt. **46**, 3332–3344 (2007).
20. D. Müller, A. Ansmann, V. Freudenthaler, K. Kandler, C. Toledano, A. Hiebsch, J. Gasteiger, M. Esselborn, M. Tesche, B. Heese, D. Althausen, B. Weinzierl, A. Petzold, and W. von Hoyningen-Huene, "Mineral dust observed with AERONET Sun photometer, Raman lidar, and in situ instruments during SAMUM 2006: shape-dependent particle properties," J. Geophys. Res. **115**, 1–11 (2010).
21. A. Fedarenka, O. Dubovik, P. Goloub, Z. Q. Li, T. Lapyonok, P. Litvinov, L. Barel, L. Gonzalez, T. Podvin, and D. Crozel, "Utilization of AERONET polarimetric measurements for improving retrieval of aerosol microphysics: GSFC, Beijing and Dakar data analysis," J. Quant. Spectrosc. Radiat. Transfer **179**, 72–97 (2016).
22. M. Kahnert, T. Nousiainen, and H. Lindqvist, "Review: model particles in atmospheric optics," J. Quant. Spectrosc. Radiat. Transfer **146**, 41–58 (2014).
23. T. Nousiainen, M. Kahnert, and H. Lindqvist, "Can particle shape information be retrieved from light-scattering observations using spheroidal model particles?" J. Quant. Spectrosc. Radiat. Transfer **112**, 2213–2225 (2011).
24. J. Wang, X. Liu, S. A. Christopher, J. S. Reid, E. Reid, and H. Maring, "The effects of non-sphericity on geostationary satellite retrievals of dust aerosols," Geophys. Res. Lett. **30**, 2293 (2003).
25. T. Nousiainen, M. Kahnert, and B. Veihelmann, "Light scattering modeling of small feldspar aerosol particles using polyhedral prisms and spheroids," J. Quant. Spectrosc. Radiat. Transfer **101**, 471–487 (2006).
26. T. Nousiainen, O. Muñoz, H. Lindqvist, P. Mauno, and G. Videen, "Light scattering by large Saharan dust particles: comparison of modeling and experimental data for two samples," J. Quant. Spectrosc. Radiat. Transfer **112**, 420–433 (2011).
27. M. Kahnert, T. Nousiainen, and P. Mauno, "On the impact of nonsphericity and small-scale surface roughness on the optical properties of hematite aerosols," J. Quant. Spectrosc. Radiat. Transfer **112**, 1815–1824 (2011).
28. L. Lorenz, "Lysbevegelser i og uden for en af plane Lysbolger belyst Kugle. Det kongelig danske Videnskabernes Selskabs Skrifter," Naturvidenskab. Math. Afd. **VI**, 2–62 (1890).
29. G. Mie, "Beiträge zur Optik trüber Medien, speziell kolloidaler Metallösungen," Ann. Phys., Vierte Folge **25**, 377–445 (1908).
30. P. Debye, "Der Lichtdruck auf Kugeln von beliebigem," Material. Ann. Phys. **335**, 57–136 (1909).
31. M. I. Mishchenko and L. D. Travis, "Capabilities and limitations of a current Fortran implementation of the T-matrix method for randomly oriented, rotationally symmetric scatterers," J. Quant. Spectrosc. Radiat. Transfer **60**, 309–324 (1998).
32. M. A. Yurkin and A. G. Hoekstra, "User manual for the discrete dipole approximation code ADDA 1.1," (2012), http://a-dda.googlecode.com/svn/tags/rel_1.1/doc/manual.pdf.
33. P. Yang and K. N. Liou, "Geometric-optics-integral-equation method for light scattering by nonspherical ice crystals," Appl. Opt. **35**, 6568–6584 (1996).
34. H. G. Horváth and D. Varjú, *Polarized Light in Animal Vision* (Springer, 2004).
35. J. L. Deuze, M. Herman, and R. Santer, "Fourier series expansion of the transfer equation in the atmosphere-ocean system," J. Quant. Spectrosc. Radiat. Transfer **41**, 483–494 (1989).
36. Z. Q. Li, H. Xu, K. T. Li, D. H. Li, Y. S. Xie, L. Li, Y. Zhang, X. F. Gu, W. Zhao, Q. J. Tian, R. R. Deng, X. L. Su, B. Huang, Y. L. Qiao, W. Y. Cui, Y. Hu, C. L. Gong, Y. Q. Wang, X. F. Wang, J. P. Wang, W. B. Du, Z. Q. Pan, Z. Z. Li, and D. Bu, "Comprehensive study of optical, physical, chemical, and radiative properties of total columnar atmospheric aerosols over china: an overview of sun-sky radiometer observation network (SONET) measurements," Bull. Am. Meteor. Soc. **99**(4), 739–755 (2018).
37. O. Dubovik, B. Holben, T. F. Eck, A. Smirnov, Y. J. Kaufman, M. D. King, D. Tanré, and I. Slutsker, "Variability of absorption and optical properties of key aerosol types observed in worldwide locations," J. Atmos. Sci. **59**, 590–608 (2002).
38. A. Deepak and H. E. Gerber, "Report of the experts meeting on aerosols and their climatic effects," WCP-55, 86 (WMO, 1983).